e^+e^- PAIR PRODUCTION FROM NUCLEON TARGETS IN THE RESONANCE REGION*

Madeleine Soyeur

DAPNIA/SPhN, CEA/Saclay, 91191 Gif-sur-Yvette Cedex, France

Matthias F.M. Lutz

GSI, Planckstrasse 1, 64291 Darmstadt, Germany

(Received November 14, 2005)

We discuss two processes, the $\pi N \to e^+e^-N$ and the $\gamma N \to e^+e^-N$ reactions, below and close to the vector meson production threshold ($1.40 < \sqrt{s} < 1.75\,\mathrm{GeV}$). The aim is to gain understanding of the coupling of vector fields (associated with ρ^0- and ω-mesons) to low-lying baryon resonances. These couplings are not well-known and important for baryon structure studies and for dynamical descriptions of vector meson propagation in the nuclear medium. The e^+e^- pair production amplitudes are determined by the $\pi N \to \rho^0 N$, $\pi N \to \omega N$, $\gamma N \to \rho^0 N$ and $\gamma N \to \omega N$ amplitudes supplemented by the Vector Meson Dominance assumption. The vector meson production amplitudes are calculated consistently using a relativistic and unitary coupled-channel approach to meson–nucleon scattering. We display results showing the importance of the quantum interference between ρ^0- and ω-mesons in the e^+e^- channel to unravel the strength of the coupling of ρ^0- and ω-mesons to specific baryon excitations. The $\pi N \to e^+e^-N$ and $\gamma N \to e^+e^-N$ reactions underlie the more complex $\pi A \to e^+e^-X$ and $\gamma A \to e^+e^-X$ nuclear processes whose measurement is planned at GSI (with the HADES detector) and under analysis at JLab (with the CLAS detector).

PACS numbers: 13.20.Jf, 14.20.Gk

1. Introduction

The $\pi N \to e^+e^-N$ and the $\gamma N \to e^+e^-N$ reactions below and close to the vector meson production threshold ($1.40 < \sqrt{s} < 1.75\,\mathrm{GeV}$) are remarkable processes to study the coupling of low-lying baryon excitations to the ρ^0- and ω-meson fields. The invariant mass of the final time-like photon

* Presented at the XXIX Mazurian Lakes Conference on Physics August 30–September 6, 2005, Piaski, Poland.

can be smaller than the physical mass of the ρ^0- and ω-mesons, hence offering the possibility to study the vector field-nucleon transition couplings of baryon resonances of masses smaller than 1.72 GeV (the vector meson–nucleon threshold energy). This possibility relies on the Vector Meson Dominance of the electromagnetic current, an assumption expected to be valid in the vicinity of the vector meson poles [1, 2]. Another important property of these reactions is the ρ^0–ω interference in the e^+e^- channel. This effect is large in the kinematics under consideration and generates patterns in the e^+e^- pair invariant mass distributions linked to the resonant structure of the amplitudes. These large interferences can be destructive or constructive, in such a way that the mere magnitude of the cross sections in a given range of total center of mass energy provides by itself a strong constraint on the underlying, mostly resonant dynamics.

The interest of our study lies in the availability of detector systems able to reject the hadronic backgrounds and to measure the small cross sections expected for dilepton production in πN and γN reactions. The $\pi N \to e^+e^- N$ reaction could be studied at GSI with the HADES detector and the secondary pion beam [3,4]. The $\gamma N \to e^+e^- N$ reaction could be measured with the CLAS detector at JLab, where inclusive e^+e^- pair production data on deuteron and nuclear targets have been taken recently (G7 experiment) [5].

We discuss briefly the processes building up the amplitudes for the $\pi N \to e^+e^- N$ and $\gamma N \to e^+e^- N$ reactions and the way they are calculated in Sec. 2. We show numerical results for the $\pi^- p \to e^+e^- n$ and $\pi^+ n \to e^+e^- p$ reactions in Sec. 3 and for the $\gamma p \to e^+e^- p$ and $\gamma n \to e^+e^- n$ reactions in Sec. 4. We conclude by a few comments in Sec. 5. The work outlined in this paper relies on two published articles [6, 7].

2. The $\pi N \to e^+e^- N$ and $\gamma N \to e^+e^- N$ amplitudes

The graphs entering the calculation of the $\pi N \to e^+e^- N$ and $\gamma N \to e^+e^- N$ amplitudes are displayed in Figs. 1 and 2.

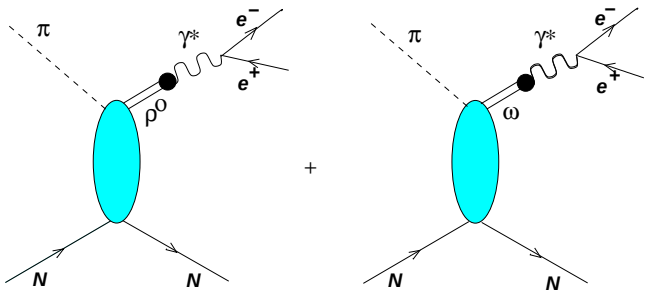


Fig. 1. Diagrams contributing to the amplitude for the $\pi N \to e^+e^- N$ reaction.

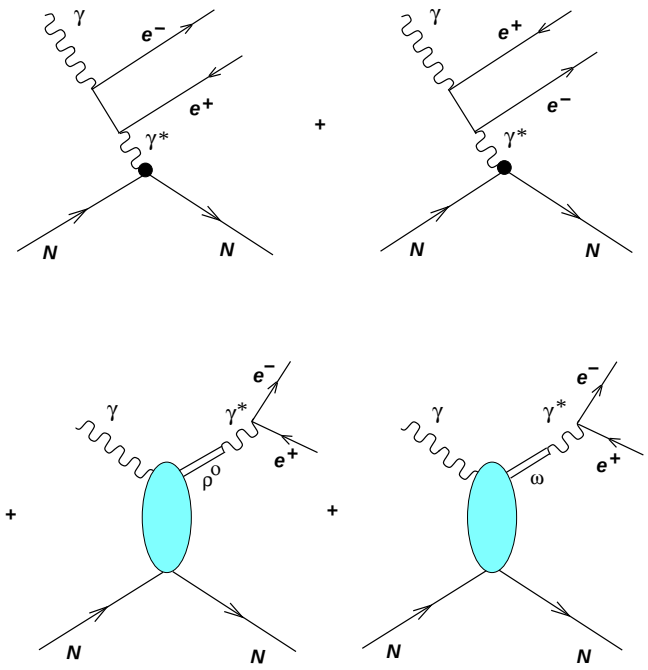


Fig. 2. Diagrams contributing to the amplitude for the $\gamma N \to e^+e^-N$ reaction.

For the $\pi N \to e^+e^-N$ reaction, the amplitude consists of two terms representing the production of a massive photon of isovector and isoscalar character, respectively. These massive photons can be related to the ρ^0- and ω-meson fields using the Vector Meson Dominance assumption [1, 2]. For the $\gamma N \to e^+e^-N$ reaction, there are four terms. The first two diagrams are associated with the electromagnetic production of e^+e^- pairs (Bethe–Heitler processes). They depend on the (well-known) nucleon electromagnetic form factors at low momentum transfers. The last two diagrams, analogous to the graphs of Fig. 1 for the $\pi N \to e^+e^-N$ reaction, represent the photoproduction of isovector and isoscalar massive photons in the Vector Meson Dominance model.

The main dynamical quantities entering the calculation of the $\pi N \to e^+e^-N$ and $\gamma N \to e^+e^-N$ cross sections are, therefore, the $\pi N \to \rho N$, $\pi N \to \omega N$, $\gamma N \to \rho N$ and $\gamma N \to \omega N$ amplitudes. They are computed using the relativistic, chiral coupled-channel approach of Ref. [8]. This model offers a consistent picture of the πN and γN reactions and involves the πN, $\pi\Delta$, ρN, ωN, $K\Lambda$, $K\Sigma$ and ηN hadronic channels. It is restricted to center of mass energies ranging between 1.40 GeV and 1.75 GeV and describes vector meson–nucleon channels below and very close to the vector meson threshold ($\sqrt{s} \simeq 1.72$ GeV). The vector meson and the nucleon in the

final state are assumed to be in relative S-wave. The Bethe–Salpeter kernel for the coupled-channel system is constructed from an effective quasi-local meson–meson-baryon–baryon Lagrangian. The fundamental fields are the photon, the mesons, the nucleon and the $\Delta(1232)$. The baryon resonances which do not belong to the large N_c groundstate multiplets are generated dynamically [9]. They are the $N(1520)$, $N(1535)$, $N(1650)$, $\Delta(1620)$ and $\Delta(1700)$ resonances. A generalized Vector Meson Dominance assumption is used to relate amplitudes involving photons to amplitudes involving vector mesons. The effective Lagrangian parameters are fitted using all available data, such as phase shifts, inelasticity parameters, pion photoproduction multipole amplitudes, inelastic pion–nucleon cross sections. The quality of the fit is quite satisfactory for all these quantities in the interval 1.40 GeV $\leq \sqrt{s} \leq$ 1.75 GeV [8].

The presence of baryon resonances in this energy range is reflected in the structure of the scattering amplitudes for vector meson production. It is this particular structure that we are interested in unraveling in e^+e^- pair production processes. We illustrate the resonant behavior of the vector meson production amplitudes by showing in Fig. 3 the (projected) amplitudes for the $\pi N \to \omega N$ process in the S11 and D13 partial waves [6]. In the S11 channel, the $N(1535)$ and the $N(1650)$ resonances lead to peak structures in the imaginary parts of the amplitudes. The pion-induced ω production amplitudes in the D13 channel reflect the strong coupling of the $N(1520)$ resonance to the ωN channel [8]. The $\pi N \to \omega N$ amplitudes contain also significant contributions from non-resonant, background terms. Similar considerations hold for the other partial waves and in general for the vector meson production amplitudes in the resonance region [6, 7].

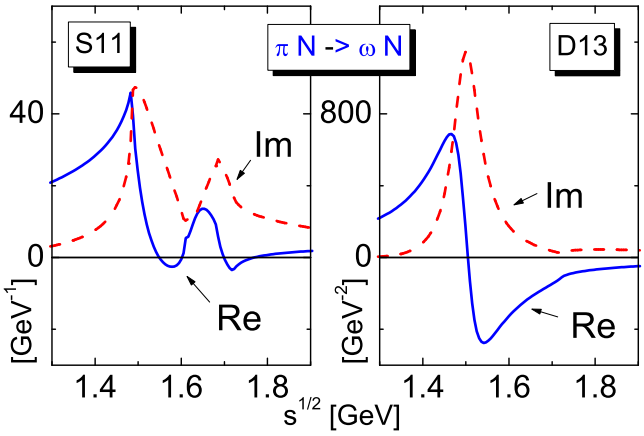


Fig. 3. Amplitudes for the $\pi N \to \omega N$ process in the S11 and D13 partial waves [6].

The $\pi N \to e^+e^-N$ and $\gamma N \to e^+e^-N$ amplitudes involving intermediate vector mesons in the final state are calculated assuming the specific Vector Meson Dominance form given by the meson–photon interaction terms,

$$\mathcal{L}_{\gamma V}^{\rm int} \;=\; \frac{f_\rho}{2M_\rho^2} F^{\mu\nu}\,\rho^0_{\mu\nu} \;+\; \frac{f_\omega}{2M_\omega^2} F^{\mu\nu}\,\omega_{\mu\nu}\,, \tag{1}$$

where the photon and vector meson field tensors are defined by $F^{\mu\nu} = \partial^\mu A^\nu - \partial^\nu A^\mu$ and $V^{\mu\nu} = \partial^\mu V^\nu - \partial^\nu V^\mu$. This particular form of the Vector Meson Dominance applies for e^+e^- pairs not too far from the vector meson pole (in contrast to the generalized Vector Meson Dominance prescription used in Ref. [8] needed for extrapolations to the photon point). In Eq. (1), M_ρ and M_ω are the ρ- and ω-masses and f_ρ and f_ω are dimensional coupling constants. Their magnitude can be determined from the e^+e^- partial decay widths of the ρ- and ω-mesons to be [10]

$$|f_\rho| \;=\; 0.036\,{\rm GeV}^2\,, \tag{2}$$

$$|f_\omega| \;=\; 0.011\,{\rm GeV}^2\,. \tag{3}$$

The relative sign of f_ρ and f_ω is fixed by the vector meson photoproduction amplitudes [8]. We assume that the phase correlation between isoscalar and isovector currents is identical for real and virtual photons as in Sakurai's realization of the Vector Meson Dominance assumption [1]. With the conventions used in this paper, both f_ρ and f_ω are real and positive.

The Bethe–Heitler terms are computed with phenomenological electromagnetic form factors [7].

Even though we plotted rather broad e^+e^- pair invariant mass spectra to illustrate general behaviours, we emphasize that our approach is valid only for values of $m_{e^+e^-}$ not too far from $(\sqrt{s} - M_N)$. This is a consequence of the assumption that the vector meson and the nucleon in the final state are in relative S-wave in the model of Ref. [8].

3. The $\pi N \to e^+e^-N$ reaction: numerical results

The differential cross sections obtained for the $\pi^-p \to e^+e^-n$ and the $\pi^+n \to e^+e^-p$ reactions at $\sqrt{s} = 1.55\,{\rm GeV}$ are shown in Figs. 4 and 5. These figures illustrate the overall behaviours of the invariant e^+e^- invariant mass spectra for these reactions below threshold. For the two reactions, the ω and ρ^0 contributions to the cross section are comparable. This property is quite remarkable in view of the Vector Meson Dominance coupling constants given in Eqs. (2) and (3) and reflect the result that the $\pi N \to \omega N$ amplitudes are much larger than the $\pi N \to \rho N$ amplitudes in the model of Ref. [8]. The ρ^0–ω interference is destructive for the $\pi^-p \to e^+e^-n$ reaction and

constructive for the $\pi^+ n \to e^+ e^- p$ process. Consequently, the $\pi^- p \to e^+ e^- n$ differential cross section is extremely small in the range of invariant masses considered in this calculation (of the order of 10 nb GeV^{-2}). In contrast, the constructive ρ^0–ω interference for the $\pi^+ n \to e^+ e^- p$ reaction leads to a sizeable differential cross section (of the order of 150 nb GeV^{-2}).

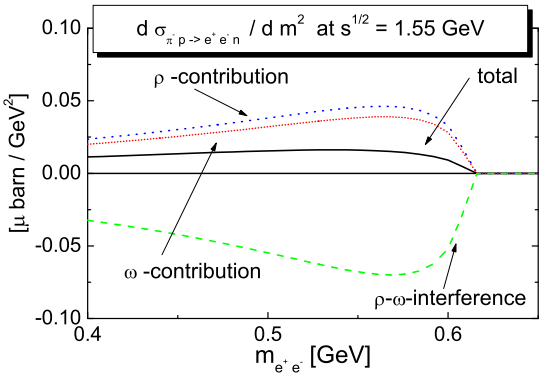


Fig. 4. Differential cross section for the $\pi^- p \to e^+ e^- n$ reaction at $\sqrt{s} = 1.55$ GeV as function of the invariant mass of the $e^+ e^-$ pair [6].

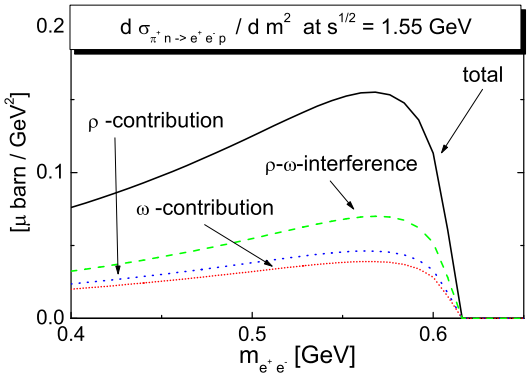


Fig. 5. Differential cross section for the $\pi^+ n \to e^+ e^- p$ reaction at $\sqrt{s} = 1.55$ GeV as function of the invariant mass of the $e^+ e^-$ pair [6].

This is a very striking prediction, linked to the resonant structure and magnitude of the scattering amplitudes. These cross sections reflect indeed the couplings of both the $N(1520)$ and $N(1535)$ baryon resonances to the vector meson–nucleon channels. Data on differential cross sections for the $\pi^- p \to e^+ e^- n$ and $\pi^+ n \to e^+ e^- p$ reactions at $\sqrt{s} = 1.55$ GeV would clearly be very useful for making progress in the understanding of these couplings.

Similar interference patterns are obtained until $\sqrt{s} = 1.70$ GeV. They are, however, sensitive to higher-lying resonances [6].

Figs. 6 and 7 display the $\pi N \to e^+e^-N$ differential cross section at $\sqrt{s} = 1.75\,\mathrm{GeV}$, *i.e.* right above the ω-meson production threshold. The interference pattern changes dramatically. The differential cross sections for the $\pi^-p \to e^+e^-n$ and $\pi^+n \to e^+e^-p$ reactions are completely dominated by the ω-contribution. The magnitudes of the cross sections for the two reactions are now comparable. The ρ^0–ω interference is still destructive in the $\pi^-p \to e^+e^-n$ channel and constructive in the $\pi^+n \to e^+e^-p$ channel, but very small. In both reactions, crossing the ω-production threshold leads to a sharp increase in the cross section, by two orders of magnitude in the $\pi^-p \to e^+e^-n$ channel and by one order of magnitude in the $\pi^+n \to e^+e^-p$ channel.

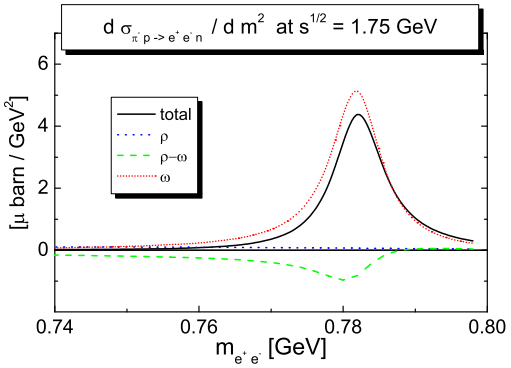


Fig. 6. Differential cross section for the $\pi^-p \to e^+e^-n$ reaction at $\sqrt{s} = 1.75\,\mathrm{GeV}$ as function of the invariant mass of the e^+e^- pair [6].

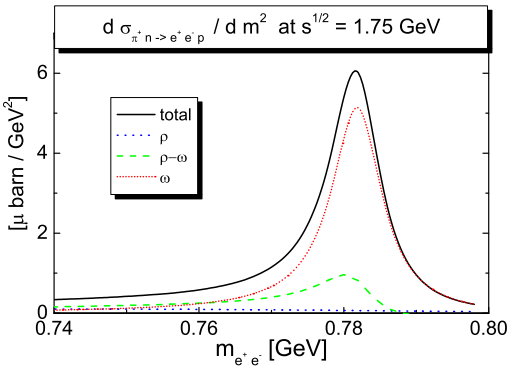


Fig. 7. Differential cross section for the $\pi^+n \to e^+e^-p$ reaction at $\sqrt{s} = 1.75\,\mathrm{GeV}$ as function of the invariant mass of the e^+e^- pair [6].

We note that the general interference pattern of the $\pi^-p \to e^+e^-n$ and $\pi^+n \to e^+e^-p$ reactions found in our calculation has also been obtained in Ref. [11], with rather different absolute magnitudes of the cross sections.

The latter result is linked to a very different prescription for the transition couplings of baryon resonances to the ρ-nucleon and ω-nucleon channels.

4. The $\gamma N \to e^+e^-N$ reaction: numerical results

We show first e^+e^- pair spectra where the leptonic phase space is fully integrated. There is no interference between Bethe–Heitler and vector meson decay amplitudes in that case [7]. Such results are presented in Fig. 8 for the $\gamma p \to e^+e^-p$ and $\gamma n \to e^+e^-n$ reactions at $\sqrt{s} = 1.55\,\text{GeV}$. To unravel the dynamics of the dilepton production process, we display separately the Bethe–Heitler and vector meson decay contributions to the cross sections and the decomposition of the vector meson decay cross sections into the ρ, ω and ρ–ω interference terms for the two possible spin channels ($J = 1/2$ and $J = 3/2$). We notice first that the Bethe–Heitler process is the dominant contribution to the differential cross sections. All experimental studies of the vector meson photoproduction amplitudes below threshold in the dilepton channel will, therefore, require a careful subtraction of the Bethe–Heitler contribution. The second observation is that the ρ-meson production and

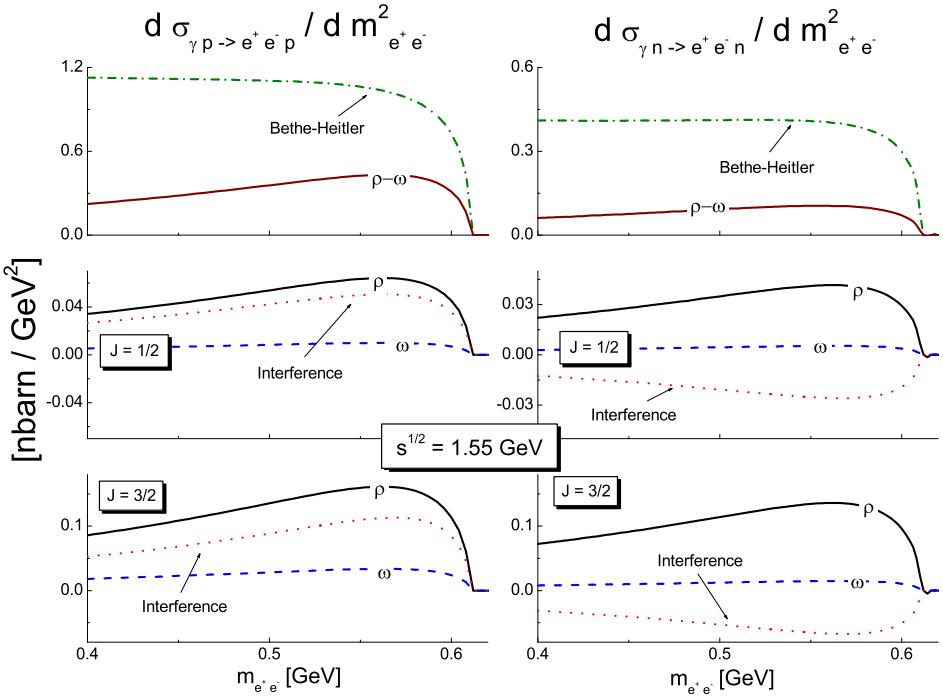


Fig. 8. Integrated spectra for the $\gamma p \to e^+e^-p$ and $\gamma n \to e^+e^-n$ reactions at $\sqrt{s} = 1.55\,\text{GeV}$ together with their different components [7].

decay into e^+e^- pairs dominates the vector meson contribution. This is expected in view of the Vector Meson Dominance coupling constants given in Eqs. (2) and (3), if no particular dynamical effect enhances the ω-meson contribution (as in the $\pi N \to e^+e^-N$ reaction). The $\gamma N \to e^+e^-N$ reaction is, therefore, a very useful process to study ρ-meson photoproduction below threshold. Thirdly we found that the quantum interference between ρ- and ω-meson e^+e^- decays is constructive for proton targets and destructive for neutron targets, in both $J = 1/2$ and $J = 3/2$ channels. The effects of this interference are, however, less pronounced than in the case of the $\pi N \to e^+e^-N$ reaction because of the relative smallness of the ω-meson contribution.

The interference of Bethe–Heitler pairs with e^+e^- pairs produced by the decay of vector mesons reflects in asymmetries [12,13]. They are defined by subdividing the lepton pair phase space into two hemispheres. Considering first the rest frame of the produced e^+e^- pair, we call forward and backward electrons those characterized by $\cos(\vec{p}_-, \vec{q}) > 0$ and $\cos(\vec{p}_-, \vec{q}) < 0$, respectively, where $q\,, p_+$ and p_- are the photon, positron and electron momenta. If the e^+e^- pair is moving, we can project the cross section onto the forward and backward hemispheres using the θ functions, $\theta[+q\,(p_+ - p_-)]$ and $\theta[-q\,(p_+ - p_-)]$ [7]. We refer to these projections as σ^+ and σ^-. The symmetric and asymmetric parts of the differential cross sections are given by

$$\left[\frac{d\sigma^{sym}}{dm_{e^+e^-}{}^2}\right]_{\gamma N\to e^+e^-N} = \left[\frac{d\sigma^{+}}{dm_{e^+e^-}{}^2}\right]_{\gamma N\to e^+e^-N} + \left[\frac{d\sigma^{-}}{dm_{e^+e^-}{}^2}\right]_{\gamma N\to e^+e^-N}, \quad (4)$$

$$\left[\frac{d\sigma^{asym}}{dm_{e^+e^-}{}^2}\right]_{\gamma N\to e^+e^-N} = \left[\frac{d\sigma^{+}}{dm_{e^+e^-}{}^2}\right]_{\gamma N\to e^+e^-N} - \left[\frac{d\sigma^{-}}{dm_{e^+e^-}{}^2}\right]_{\gamma N\to e^+e^-N}. \quad (5)$$

We restrict our discussion to the results obtained for the $\gamma\, p \to e^+e^-p$ reaction at $\sqrt{s} = 1.65$ and $1.75\,\mathrm{GeV}$, displayed in Fig. 9. We refer to [7] for a much more extended presentation. The symmetric part is the total cross section and hence the sum of the Bethe–Heitler and vector meson cross sections. The antisymmetric part reflects the interference of the Bethe–Heitler and vector meson pairs. The comparison of the symmetric and antisymmetric cross sections shows that the antisymmetric cross section is much smaller (by more than two orders of magnitude in the mass range of interest) than the symmetric cross section. The asymmetric cross section consists of terms reflecting the interference of Bethe–Heitler pairs with ρ-meson and ω-meson decay pairs, respectively. We see from Fig. 9 that the Bethe–Heitler ρ-meson interference is the dominant contribution, except for pairs arising from the decay of ω-mesons produced on the mass-shell slightly above threshold.

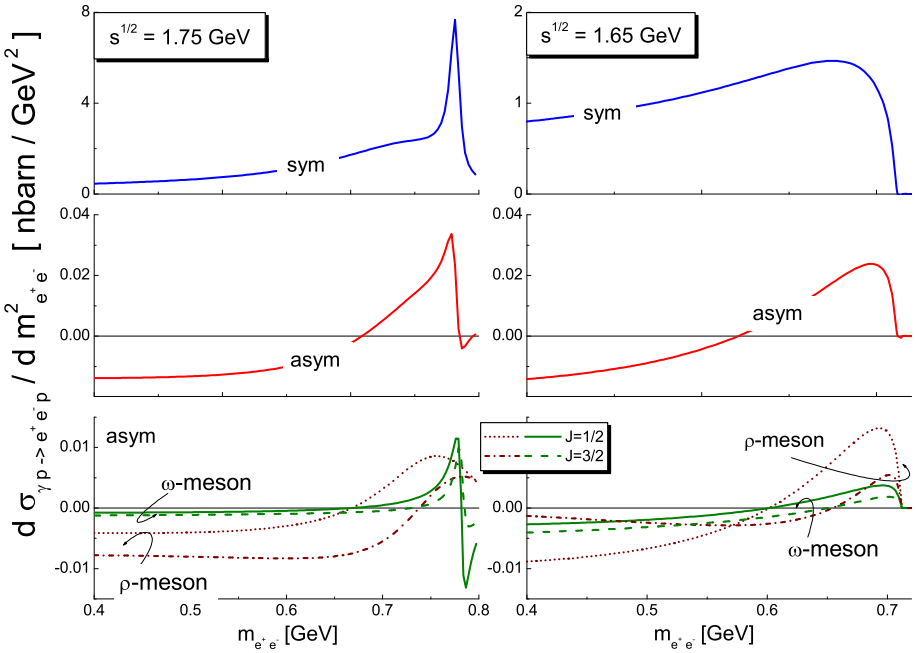


Fig. 9. Symmetric and asymmetric contributions to the $\gamma p \to e^+e^-p$ cross section at $\sqrt{s} = 1.75$ and 1.65 GeV together with their different components [7].

Angular distributions for the different subprocesses indicate that the pairs originating from Bethe–Heitler processes and vector meson decays are produced in very different regions of phase-space [7]. The Bethe–Heitler pairs are emitted at forward angles while e^+e^- pairs from vector meson decays are produced isotropically in the center of mass. The Bethe–Heitler spectra peak strongly at low e^+e^- pair invariant masses, while vector meson decay is enhanced by the proximity of the poles for large e^+e^- pair masses. Consequently the quantum interference between the two processes is very small and most significant at small angles where the Bethe–Heitler cross section is very large.

Our results suggest that the vector meson contribution can be determined quite accurately from experimental e^+e^- spectra by subtracting the Bethe–Heitler term and neglecting the small interference of Bethe–Heitler pairs with vector meson e^+e^- decays.

5. Conclusion

We have calculated consistently the $\pi N \to e^+e^-N$ and $\gamma N \to e^+e^-N$ cross sections below and just above the vector meson production threshold ($1.40 < \sqrt{s} < 1.75\,\text{GeV}$). The ρ- and ω-meson production amplitudes

underlying these processes are computed using the relativistic and unitary coupled-channel approach to meson–nucleon scattering of Ref. [8], supplemented with the Vector Dominance assumption (1) for the time-like photon in the final state.

We have found that the $\pi N \to e^+e^-N$ and $\gamma N \to e^+e^-N$ reactions are unique and complementary processes to study the couplings of selected baryon resonances to the vector meson–nucleon channels. The complementarity comes from the fact that the $\pi^-p \to e^+e^-n$ and the $\pi^+n \to e^+e^-p$ reactions are very sensitive to the couplings of selected baryon resonances to both ρ^0- and ω-mesons in our model while the $\gamma N \to e^+e^-N$ process is ideally suited to study the coupling of low-lying baryon resonances to the ρ^0-nucleon channel. The quantum interference of ρ^0- and ω-mesons in the e^+e^- channel amplifies the sensitivity of the $\pi N \to e^+e^-N$ and $\gamma N \to e^+e^-N$ reactions to the coupling of vector fields to baryon resonances.

Experimental data on both processes in the kinematics under consideration are expected in the near future, from the CLAS detector at JLab for the $\gamma N \to e^+e^-N$ reaction [5] and from the HADES detector and the secondary pion beam at GSI for the $\pi N \to e^+e^-N$ reaction [3, 4].

One of us (M.S.) is grateful to the Organizers of the XXIX Mazurian Lakes Conference on Physics for inviting her to a most pleasant and enriching meeting.

REFERENCES

[1] J.J. Sakurai, *Currents and Mesons*, The University of Chicago Press, 1969.
[2] N.M. Kroll, T.D. Lee, B. Zumino, *Phys. Rev.* **157**, 1376 (1967).
[3] W. Schön *et al., Acta Phys. Pol. B* **27**, 2959 (1996).
[4] HADES Collaboration, private communication.
[5] C. Tur, Presentation at the APS Meeting, April 16th–19th, 2005, Tampa (Florida).
[6] M.F.M. Lutz, B. Friman, M. Soyeur, *Nucl. Phys.* **A713**, 97 (2003).
[7] M.F.M. Lutz, M. Soyeur, *Nucl. Phys.* **A760**, 85 (2005).
[8] M.F.M. Lutz, Gy. Wolf, B. Friman, *Nucl. Phys.* **A706**, 431 (2002).
[9] M.F.M. Lutz, E.E. Kolomeitsev, *Found. Phys.* **31**, 1671 (2001).
[10] B. Friman, M. Soyeur, *Nucl. Phys.* **A600**, 477 (1996).
[11] A.I. Titov, B. Kämpfer, *Eur. Phys. J.* **A12**, 217 (2001).
[12] A.Yu. Korchin, O. Scholten, F. de Jong, *Phys. Lett.* **B402**, 1 (1997).
[13] A.I. L'vov *et al., Phys. Rev.* **C57**, 312 (1998).